Journal of
Mechanics of
Materials and Structures

FINITE STRAIN MICROMECHANICAL MODELING OF THERMOVISCOELASTIC MATRIX COMPOSITES

Jacob Aboudi

Volume 6, No. 1-4 January–June 2011

mathematical sciences publishers

JOURNAL OF MECHANICS OF MATERIALS AND STRUCTURES
Vol. 6, No. 1-4, 2011

msp

FINITE STRAIN MICROMECHANICAL MODELING OF THERMOVISCOELASTIC MATRIX COMPOSITES

JACOB ABOUDI

A finite strain micromechanical analysis is generalized for the modeling of thermoviscoelastic matrix composites. The thermoviscoelastic matrix of the composite is represented by a finite thermoviscoelasticity theory that permits (in contrast to finite linear thermoviscoelasticity theories) large deviations away from thermodynamic equilibrium. As a result, it is possible to subject the composite to large thermomechanical loadings. In addition, the possibility of evolving damage in the matrix is included. The derived micromechanical model is applied to investigate the behavior of a thermoviscoelastic rubber-like matrix reinforced by steel fibers in various circumstances. By subjecting the composite to mechanical loading under isentropic conditions, the micromechanical model is employed for the prediction of thermoelastic inversion point at which the Gough–Joule phenomenon at the rubber-like phase occurs. Results are given that show the effect of damage, elevated temperature and viscoelasticity of the matrix on the global response of the composite including its creep and relaxation behavior.

1. Introduction

The viscoelastic effects of polymers that are undergoing large deformations can be modeled by finite linear viscoelasticity. In the framework of this theory the strains are finite, but the deviations away from thermodynamic equilibrium are assumed to be small. This implies that the equations that control the evolution of the internal variables are linear; see [Lockett 1972; Christensen 1982; Holzapfel 2000; Simo 1987], for example. For large deviations from equilibrium the finite linear viscoelasticity is not applicable any more and nonlinear evolution laws must be introduced to allow more accurate modeling. To this end a finite viscoelasticity theory was formulated in [Reese and Govindjee 1998b] in which the equations of evolution are nonlinear thus allowing very large strains to take place. In [Govindjee and Reese 1997] comparisons have been made between the finite linear viscoelasticity of [Simo 1987] and their developed finite viscoelasticity theory.

The development of thermoviscoelasticity theories at finite strain that include viscous and nonisothermal effects is very important since the behavior of polymeric materials is strongly influenced by temperature changes. A thermoviscoelasticity theory at finite strains was presented in [Holzapfel and Simo 1996]. In this formulation, however, the evolution equations of the internal variables are linear and, therefore, this theory can be considered as finite linear thermoviscoelasticity. Finite thermoviscoelasticity theories that allow finite perturbations away from thermodynamic equilibrium were presented by [Lion 1996; Reese

Keywords: finite thermoviscoelasticity, large deformations, Rubber-like matrix composites, evolving damage, finite strain high-fidelity generalized method of cells.

and Govindjee 1998a]. The formulation in the latter reference is based on entropic elasticity and involves nonlinear evolution equations that allow the modeling of significant thermomechanical deformations of the material and permits large deformation rates.

The derived constitutive equations of [Reese and Govindjee 1998a] are based on the multiplicative decomposition of the deformation gradient into elastic and viscous parts. In addition, the free energy is decomposed into equilibrium (which corresponds to time-independent thermoelastic deformation) and nonequilibrium (which corresponds to the time-dependent deformation) parts. Damage considerations are not included in the finite thermoviscoelasticity of that paper. In the present investigation, evolving damage in finite thermoviscoelastic materials is included by adopting, in the framework of continuum damage mechanics, the derivation of [Lin and Schomburg 2003; Miehe and Keck 2000], according to which the rate of damage depends upon the kinematic arc-length. Isothermal finite viscoelasticity with evolving damage is obtained as a special case, and by neglecting the thermal and viscous effects, the special case of a hyperelastic material with evolving damage is obtained.

In [Aboudi 2004], a micromechanical analysis was proposed for the prediction of the behavior of composites undergoing large deformations in which one of the phases is modeled by the finite linear thermoviscoelasticity theory of [Holzapfel and Simo 1996]. In the present investigation, this finite strain micromechanical analysis, referred to as *high-fidelity generalized method of cells* (HFGMC), is extended to incorporate polymeric phases that can be modeled by the finite thermoviscoelasticity of [Reese and Govindjee 1998a] in which damage can evolve, the rate of which depends upon the kinematic arc-length. As a result of the present generalization, finite strain constitutive equations that govern the macroscopic behavior of the anisotropic thermoviscoelasticity composites undergoing large deformations with evolving damage in the polymeric phase are established. These equations involve the damaged instantaneous mechanical and thermal tangent tensors as well as a global tensor that includes the current viscoelasticity and damage effects. Every one of these three tensors is given by closed-form expressions that involve the instantaneous properties of the phases and the corresponding current mechanical, thermal and viscoelastic-damage tensors which have been established from the micromechanical procedure. The special case of composites that consist of finite viscoelastic phases has been recently investigated in [Aboudi 2010].

Results are given for a thermoviscoelastic rubber-like matrix reinforced by thermoelastic steel fibers. The thermoviscoelastic rubber-like matrix consists of a system of a thermoelastic element together with a single Maxwell element which is represented by the equilibrium and the nonequilibrium parts of the free energy. The thermoelastic inversion point which is characteristic for rubber-like materials at which the Gough–Joule effect occurs is determined by analyzing an isentropic process that provides the induced temperature by stretching the composite in the transverse direction (perpendicular to the fibers). In addition, the effects of elevated temperature, viscoelasticity and damage on the steel/rubber-like composite response to mechanical and thermal loading-unloading conditions are examined, as well as its creep and relaxation behavior.

This paper is organized as follows. After a brief summary in Section 2 of the thermoviscoelastic model of [Reese and Govindjee 1998a] for monolithic materials and its coupling with evolving damage, the HFGMC analysis is described in Section 3. Section 4 includes the application of the finite strain thermoviscoelastic composite model in various circumstances, followed by conclusions and suggestions for future research.

2. Finite strain thermoviscoelasticity coupled with damage model of monolithic materials

In the present section we briefly present the constitutive behavior of finite strain thermoviscoelastic polymeric materials that exhibit evolving damage. The presentation follows the papers of [Reese and Govindjee 1998a] where no damage is accounted to and [Lin and Schomburg 2003] where evolving damage is included. The present thermoviscoelastic modeling allows finite strain and large deviations from the thermodynamic equilibrium state.

Let $\boldsymbol{X}$ and $\boldsymbol{x}$ denote the location of a point in the material with respect to the initial (Lagrangian) and current systems of coordinates, respectively, and t is the time. In terms of the local deformation gradient tensor $\boldsymbol{F}(\boldsymbol{X}, t)$, $d\boldsymbol{x} = \boldsymbol{F}(\boldsymbol{X}, t)d\boldsymbol{X}$. The deformation gradient $\boldsymbol{F}$ is expressed by the multiplicative decomposition

$$\boldsymbol{F}(\boldsymbol{X}, t) = \boldsymbol{F}^e(\boldsymbol{X}, t)\boldsymbol{F}^v(\boldsymbol{X}, t), \tag{1}$$

where $\boldsymbol{F}^e$ and $\boldsymbol{F}^v$ are the elastic and viscous parts. The Jacobians that correspond to $\boldsymbol{F}$ and $\boldsymbol{F}^e$ are: $J = \det \boldsymbol{F}$ and $J^e = \det \boldsymbol{F}^e$, respectively.

The modeling that is presented herein is based on a single Maxwell and elastic elements, but it can be extended to include several Maxwell elements. The total free energy per unit reference volume is decomposed into equilibrium (EQ) which represents the strain energy of the elastic element and a nonequilibrium (NEQ) part that accounts for the Maxwell element:

$$\psi = \psi^{\mathrm{EQ}} + \psi^{\mathrm{NEQ}}. \tag{2}$$

The equilibrium part is given by

$$\psi^{\mathrm{EQ}} = (1 - D)\left[f_{\mathrm{EQ}}\psi_0^{\mathrm{EQ}} + (e_0)_{\mathrm{EQ}}\left(1 - \frac{\theta}{\theta_0}\right) + c_0\left(\theta - \theta_0 - \theta \log \frac{\theta}{\theta_0}\right)\right], \tag{3}$$

where D denotes the amount of damage such that $0 \le D \le 1$, θ and θ_0 are the current and reference temperatures, respectively, and c_0 is the heat capacity. In this relation f_{EQ} and $(e_0)_{\mathrm{EQ}}$ are of the form

$$f_{\mathrm{EQ}} = \frac{\theta}{\theta_0}, \qquad (e_0)_{\mathrm{EQ}} = K^e\alpha^e \log J\theta_0, \tag{4}$$

where K^e and α^e are the bulk modulus and thermal expansion coefficient, respectively, of the elastic element. It follows from (3) that ψ_0^{EQ} is the equilibrium part of the free energy at the reference temperature θ_0 in the presence of damage.

The nonequilibrium part is given by

$$\psi^{\mathrm{NEQ}} = (1 - D)\left[f_{\mathrm{NEQ}}\psi_0^{\mathrm{NEQ}} + (e_0)_{\mathrm{NEQ}}\left(1 - \frac{\theta}{\theta_0}\right)\right], \tag{5}$$

where

$$f_{\mathrm{NEQ}} = \frac{\theta}{\theta_0} \quad \text{and} \quad (e_0)_{\mathrm{NEQ}} = K^v\alpha^v \log J_e\theta_0, \tag{6}$$

K^v and α^v being the bulk modulus and thermal expansion coefficient, respectively, of the viscous part of the material. Here too, $\psi^{\mathrm{NEQ}} = \psi_0^{\mathrm{NEQ}}$ for $\theta = \theta_0$ and $D \neq 0$.

The Kirchhoff stresses can be derived from the free-energy expressions above:

$$\tau^{\mathrm{EQ}} = 2\boldsymbol{F}\frac{\partial \psi^{\mathrm{EQ}}}{\partial \boldsymbol{C}}\boldsymbol{F}^T \equiv (1-D)\tau_0^{\mathrm{EQ}}, \tag{7}$$

$\boldsymbol{C} = \boldsymbol{F}^T\boldsymbol{F}$ being the right Cauchy–Green deformation tensor, and

$$\tau^{\mathrm{NEQ}} = 2\boldsymbol{F}\frac{\partial \psi^{\mathrm{NEQ}}}{\partial \boldsymbol{C}}\boldsymbol{F}^T = 2\boldsymbol{F}^e\frac{\partial \psi^{\mathrm{NEQ}}}{\partial \boldsymbol{C}^e}\boldsymbol{F}^{eT} \equiv (1-D)\tau_0^{\mathrm{NEQ}}, \tag{8}$$

where $\boldsymbol{C}^e = \boldsymbol{F}^{eT}\boldsymbol{F}^e$ and τ_0^{EQ}, τ_0^{NEQ} correspond to the Kirchhoff stresses of the undamaged material.

Let the left Cauchy–Green tensor $\boldsymbol{B} = \boldsymbol{F}\boldsymbol{F}^T$ be represented in terms of its eigenvalues b_p and unit principal directions $\boldsymbol{e}_p$, $p = 1, 2, 3$:

$$\boldsymbol{B} = \mathrm{diag}\,[b_1, b_2, b_3], \qquad \text{i.e.,} \quad \boldsymbol{B} = \sum_{p=1}^{3} b_p\, \boldsymbol{e}_p \otimes \boldsymbol{e}_p. \tag{9}$$

With $J = \det \boldsymbol{F} = \sqrt{b_1 b_2 b_3}$, the volume preserving tensor $\bar{\boldsymbol{B}} = J^{-2/3}\boldsymbol{B}$ can be accordingly represented in the form

$$\bar{\boldsymbol{B}} = \mathrm{diag}\,[\bar{b}_1, \bar{b}_2, \bar{b}_3] = (b_1 b_2 b_3)^{-1/3}\ \mathrm{diag}\,[b_1, b_2, b_3]. \tag{10}$$

The finite strain isothermal contribution ψ_0^{EQ} can be modeled by the Ogden's compressible material representation [Ogden 1984; Holzapfel 2000] as follows

$$\psi_0^{\mathrm{EQ}} = \sum_{p=1}^{3} \frac{\mu_p^e}{\alpha_p^e}\left((\bar{b}_1)^{\alpha_p^e/2} + (\bar{b}_2)^{\alpha_p^e/2} + (\bar{b}_3)^{\alpha_p^e/2} - 3\right) + \frac{K^e}{4}\left(J^2 - 2\log J - 1\right), \tag{11}$$

where μ_p^e and α_p^e are material parameters of the elastic element.

For Maxwell's element, the isothermal free energy ψ_0^{NEQ} is represented by [Reese and Govindjee 1998a]:

$$\psi_0^{\mathrm{NEQ}} = \sum_{p=1}^{3} \frac{\mu_p^v}{\alpha_p^v}\left((\bar{b}_1^e)^{\alpha_p^v/2} + (\bar{b}_2^e)^{\alpha_p^v/2} + (\bar{b}_3^e)^{\alpha_p^v/2} - 3\right) + \frac{K^v}{4}\left((J^e)^2 - 2\log J^e - 1\right), \tag{12}$$

where

$$\boldsymbol{B}^e = \boldsymbol{F}^e[\boldsymbol{F}^e]^T = \mathrm{diag}\,[b_1^e, b_2^e, b_3^e] \tag{13}$$

and $J^e = \sqrt{b_1^e b_2^e b_3^e}$, $\bar{b}_A^e = (J^e)^{-2/3} b_A^e$, and μ_p^v, α_p^v, are material parameters.

The entropy of the system can be determined from

$$\begin{aligned}
\eta &= -\frac{\partial \psi}{\partial \theta} = -\frac{\partial \psi^{\mathrm{EQ}}}{\partial \theta} - \frac{\partial \psi^{\mathrm{NEQ}}}{\partial \theta} \\
&= -(1-D)\left[\frac{1}{\theta_0}\psi_0^{\mathrm{EQ}} - \frac{1}{\theta_0}(e_0)_{\mathrm{EQ}} - c_0 \log\frac{\theta}{\theta_0}\right] - (1-D)\left[\frac{1}{\theta_0}\psi_0^{\mathrm{NEQ}} - \frac{1}{\theta_0}(e_0)_{\mathrm{NEQ}}\right] \\
&\equiv (1-D)\eta_0.
\end{aligned} \tag{14}$$

The evolution equation for the internal variables is given in [Reese and Govindjee 1998a]:

$$-\frac{1}{2}L_v[\boldsymbol{B}^e][\boldsymbol{B}^e]^{-1} = \frac{1}{2\eta_D}\mathrm{dev}\,[\tau^{\mathrm{NEQ}}] + \frac{1}{9\eta_V}\mathrm{trace}\,[\tau^{\mathrm{NEQ}}], \tag{15}$$

where η_D and η_V are the deviatoric and volumetric viscosities, respectively, and $L_v[\boldsymbol{B}^e]$, the Lie derivative of $\boldsymbol{B}^e$, can be expressed as

$$L_v[\boldsymbol{B}^e] = \boldsymbol{F}\dot{\boldsymbol{C}}^{v-1}\boldsymbol{F}^T, \tag{16}$$

with $\boldsymbol{C}^v = \boldsymbol{F}^{vT}\boldsymbol{F}^v$. For elastic bulk behavior, $1/\eta_V = 0$ and the relaxation time is given by $\xi = \eta_D/\mu$ where μ is the small strain shear modulus of the Maxwell element (the nonequilibrium part).

The integration of the evolution equation (15) is performed by means of the return mapping algorithm in conjunction with the logarithmic strain and the backward exponential approximation which were developed in the framework of elastoplasticity, see [Weber and Anand 1990; Eterovic and Bathe 1990; Cuitino and Ortiz 1992; Simo 1992]. Thus, by employing the exponential mapping algorithm, (15) is reduced to

$$\epsilon^e_{n+1,A} = \epsilon^{e\ \text{trial}}_{n+1,A} - \Delta t\left[\frac{1}{2\eta_D}\text{dev}\,[\tau^{\text{NEQ}}_A] + \frac{1}{9\eta_V}\text{trace}\,[\tau^{\text{NEQ}}]\right]_{n+1}, \tag{17}$$

with $A = 1, 2, 3$, where the principal values of the elastic logarithmic strain ϵ^e_A are given by $\epsilon^e_A = \frac{1}{2}\log b^e_A$ and Δt is the time increment between the current and previous step. In (17), the trial values of $\epsilon^{e\ \text{trial}}_{n+1,A}$ can be expressed in terms of the eigenvalues $b^{e\ \text{trial}}_{n+1,A}$ of $\boldsymbol{B}^{e\ \text{trial}}_{n+1}$ namely, $\epsilon^{e\ \text{trial}}_{n+1,A} = \frac{1}{2}\log b^{e\ \text{trial}}_{A,n+1}$, where

$$\boldsymbol{B}^{e\ \text{trial}}_{n+1} = \boldsymbol{f}_{n+1}\boldsymbol{B}^e_n\boldsymbol{f}^T_{n+1}, \tag{18}$$

with

$$\boldsymbol{f}_{n+1} = \boldsymbol{F}_{n+1}\boldsymbol{F}^{-1}_n, \tag{19}$$

Equation (17) forms a system of coupled nonlinear equations in the unknowns $\epsilon^e_{n+1,A}$, $A = 1, 2, 3$. It can be rewritten in terms of the elastic logarithmic strain increments in the form

$$\Delta\epsilon^e_A = \epsilon^{e\ \text{trial}}_{n+1,A} - \epsilon^e_{n,A} - \Delta t\left[\frac{1}{2\eta_D}\text{dev}\,[\tau^{\text{NEQ}}_A] + \frac{1}{9\eta_V}\text{trace}\,[\tau^{\text{NEQ}}]\right]_{n+1}. \tag{20}$$

In this equation, the principal values of τ^{NEQ} are given according to (8) by

$$\tau^{\text{NEQ}}_A = 2\frac{\partial\psi^{\text{NEQ}}}{\partial b_A}b_A = 2\frac{\partial\psi^{\text{NEQ}}}{\partial b^e_A}b^e_A. \tag{21}$$

The rate of damage evolution is given by (see [Lin and Schomburg 2003; Miehe and Keck 2000])

$$\dot{D} = \frac{\dot{z}}{\eta_{\text{dam}}}(D^\infty - D), \tag{22}$$

where the rate of kinematic arc length is defined by

$$\dot{z} = \sqrt{\tfrac{2}{3}}\|\dot{\boldsymbol{H}}\|, \qquad \boldsymbol{H} = \tfrac{1}{2}\log\boldsymbol{C}, \tag{23}$$

with the saturation value

$$D^\infty = \frac{1}{1 + D^\infty_0\exp\left(-\beta_{\text{dam}}/\alpha_{\text{dam}}\right)} \tag{24}$$

and

$$\beta_{\text{dam}} = \max_{0\le\xi\le t}\sqrt{\tfrac{2}{3}}\|\boldsymbol{H}(\xi)\|. \tag{25}$$

In these relations, η_{dam}, D^∞_0 and α_{dam} are material parameters.

The incremental form of the constitutive equations of the finite thermoviscoelastic material and the corresponding instantaneous tangent tensor that are needed in the following micromechanical analysis, are determined as follows. From (8) the following expression can be established

$$\Delta\tau_A^{\mathrm{NEQ}} = (1-D)\Delta\tau_{0A}^{\mathrm{NEQ}} - \tau_{0A}^{\mathrm{NEQ}}\Delta D. \tag{26}$$

Let the second-order tensor $\boldsymbol{M}^{\mathrm{NEQ}}$ be defined by

$$\boldsymbol{M}^{\mathrm{NEQ}} = [M_{AB}^{\mathrm{NEQ}}] \equiv \left[\frac{\partial \tau_{0A}^{\mathrm{NEQ}}}{\partial \epsilon_B^e}\right], \qquad A, B = 1, 2, 3, \tag{27}$$

In addition, the components of the thermal stress vector Γ^{NEQ} are determined from

$$\Gamma_A^{\mathrm{NEQ}} = -\frac{\partial \tau_{0A}^{\mathrm{NEQ}}}{\partial \theta}, \qquad A = 1, 2, 3. \tag{28}$$

In conjunction with (20), we obtain from (26) that

$$\Delta\tau_A^{\mathrm{NEQ}} = (1-D)M_{AB}^{\mathrm{NEQ}}\left\{\epsilon_{n+1,B}^{e\ \mathrm{trial}} - \epsilon_{n,B}^e - \Delta t\left[\frac{1}{2\eta_D}\mathrm{dev}\,[\tau_B^{\mathrm{NEQ}}] + \frac{1}{9\eta_V}\mathrm{trace}\,[\tau^{\mathrm{NEQ}}]\right]_{n+1}\right\} - (1-D)\Gamma_A^{\mathrm{NEQ}}\Delta\theta - \tau_{0A}^{\mathrm{NEQ}}\Delta D. \tag{29}$$

Let $\Delta\epsilon_A^e$ and $\Delta\epsilon_A^{\mathrm{ved}}$ be defined by

$$\begin{aligned}\Delta\epsilon_A &\equiv \epsilon_{n+1,A}^{e\ \mathrm{trial}} - \epsilon_{n,A}^e,\\ \Delta\epsilon_A^{\mathrm{ved}} &\equiv \Delta t\left[\frac{1}{2\eta_D}\mathrm{dev}\,[\tau_A^{\mathrm{NEQ}}] + \frac{1}{9\eta_V}\mathrm{trace}\,[\tau^{\mathrm{NEQ}}]\right]_{n+1} + [M^{\mathrm{NEQ}}]_{AB}^{-1}\tau_{0B}^{\mathrm{NEQ}}\frac{\Delta D}{1-D}.\end{aligned} \tag{30}$$

Therefore (29) can be represented by

$$\begin{aligned}\Delta\tau_A^{\mathrm{NEQ}} &= (1-D)\left\{M_{AB}^{\mathrm{NEQ}}[\Delta\epsilon_B - \Delta\epsilon_B^{\mathrm{ved}}] - \Gamma_A^{\mathrm{NEQ}}\Delta\theta\right\}\\ &\equiv (1-D)[M_{AB}^{\mathrm{NEQ}}\Delta\epsilon_B - \Gamma_A^{\mathrm{NEQ}}\Delta\theta] - \Delta W_A^{\mathrm{NEQ}},\end{aligned} \tag{31}$$

where the components $\Delta W_A^{\mathrm{NEQ}}$ involve the thermoviscoelastic and damage effects.

The fourth-order tangent tensor $\boldsymbol{d}^{\mathrm{NEQ}}$ is defined by

$$\boldsymbol{d}^{\mathrm{NEQ}} = 2\frac{\partial \boldsymbol{S}^{\mathrm{NEQ}}}{\partial \boldsymbol{C}} = 4\frac{\partial^2 \psi^{\mathrm{NEQ}}}{\partial \boldsymbol{C}\partial \boldsymbol{C}}, \tag{32}$$

where $\boldsymbol{S}^{\mathrm{NEQ}}$ is the second Piola–Kirchhoff stress tensor:

$$\boldsymbol{S}^{\mathrm{NEQ}} = 2\frac{\partial \psi^{\mathrm{NEQ}}}{\partial \boldsymbol{C}} = 2[\boldsymbol{F}^v]^{-1}\frac{\partial \psi^{\mathrm{NEQ}}}{\partial \boldsymbol{C}^e}[\boldsymbol{F}^v]^{-T}, \tag{33}$$

whose the principal values are given by

$$S_A^{\mathrm{NEQ}} = 2\frac{\partial \psi^{\mathrm{NEQ}}}{\partial b_A} = \frac{2}{b_A^v}\frac{\partial \psi^{\mathrm{NEQ}}}{\partial b_A^e}, \qquad A = 1, 2, 3, \tag{34}$$

with $b_A^v = b_A/b_A^e$ being the principal values of $\boldsymbol{B}^v = \boldsymbol{F}^v[\boldsymbol{F}^v]^T = \text{diag}\,[b_1^v, b_2^v, b_3^v]$. The principal values of $\boldsymbol{d}^{\text{NEQ}}$ can be determined from the following expression [Holzapfel 2000]:

$$\boldsymbol{d}^{\text{NEQ}} = \sum_{A=1}^{3}\sum_{B=1}^{3} \frac{1}{\lambda_B}\frac{\partial S_A^{\text{NEQ}}}{\partial \lambda_B} \boldsymbol{N}_A \otimes \boldsymbol{N}_A \otimes \boldsymbol{N}_B \otimes \boldsymbol{N}_B + \sum_{A=1}^{3}\sum_{B\neq A=1}^{3} \frac{S_B^{\text{NEQ}} - S_A^{\text{NEQ}}}{(\lambda_B)^2 - (\lambda_A)^2}(\boldsymbol{N}_A \otimes \boldsymbol{N}_B \otimes \boldsymbol{N}_A \otimes \boldsymbol{N}_B + \boldsymbol{N}_A \otimes \boldsymbol{N}_B \otimes \boldsymbol{N}_B \otimes \boldsymbol{N}_A), \quad (35)$$

where

$$\frac{1}{\lambda_B}\frac{\partial S_A^{\text{NEQ}}}{\partial \lambda_B} = 2\frac{\partial S_A^{\text{NEQ}}}{\partial b_B} = \frac{4}{b_A^v b_B^v}\frac{\partial^2 \psi^{\text{NEQ}}}{\partial b_A^e b_B^e}, \quad (36)$$

with $\lambda_A = \sqrt{b_A}$ and $\boldsymbol{N}_A$ denotes the principal referential orthonormal directions. It should be noted that for $\lambda_A = \lambda_B$, a Taylor expansion shows that

$$\lim_{\lambda_B \to \lambda_A} \frac{S_B^{\text{NEQ}} - S_A^{\text{NEQ}}}{(\lambda_B)^2 - (\lambda_A)^2} = \frac{1}{2\lambda_B}\left[\frac{\partial S_B^{\text{NEQ}}}{\partial \lambda_B} - \frac{\partial S_A^{\text{NEQ}}}{\partial \lambda_B}\right]. \quad (37)$$

The second-order thermal stress tensor γ^{NEQ} is determined from

$$\gamma^{\text{NEQ}} = -\frac{\partial \boldsymbol{S}^{\text{NEQ}}}{\partial \theta} = -2\frac{\partial^2 \psi^{\text{NEQ}}}{\partial \boldsymbol{C}\,\partial \theta} \quad (38)$$

and its principal values are given by

$$\gamma_A^{\text{NEQ}} = -2\frac{\partial^2 \psi^{\text{NEQ}}}{\partial b_A \partial \theta} = -\frac{2}{b_A^v}\frac{\partial^2 \psi^{\text{NEQ}}}{\partial b_A^e \partial \theta}. \quad (39)$$

The values of γ_A^{NEQ} can be readily related to Γ_A^{NEQ} in (28) by employing the relation: $\tau = \boldsymbol{F}\boldsymbol{S}\boldsymbol{F}^T$ from which the equality $\Gamma_A^{\text{NEQ}} = b_A \gamma_A^{\text{NEQ}}$ is obtained.

The fourth-order first tangent tensor $\boldsymbol{R}^{\text{NEQ}}$ which is defined by

$$\boldsymbol{R}^{\text{NEQ}} = \frac{\partial \boldsymbol{T}^{\text{NEQ}}}{\partial \boldsymbol{F}}, \quad (40)$$

where $\boldsymbol{T}^{\text{NEQ}}$ is the first Piola–Kirchhoff stress tensor, can be determined from

$$\boldsymbol{R}^{\text{NEQ}} = \boldsymbol{F}\,\boldsymbol{d}^{\text{NEQ}}\,\boldsymbol{F}^T + \boldsymbol{S}^{\text{NEQ}} \otimes \boldsymbol{I}, \quad (41)$$

with $\boldsymbol{I}$ denoting the unit second-order tensor. Thus, the rate form of the nonequilibrium portion of the constitutive equations of the finite thermoviscoelastic material is given by

$$\dot{\boldsymbol{T}}^{\text{NEQ}} = \boldsymbol{R}^{\text{NEQ}} : \dot{\boldsymbol{F}} - \boldsymbol{H}^{\text{NEQ}}\dot{\theta} - \dot{\boldsymbol{V}}^{\text{NEQ}}, \quad (42)$$

where by taking into account the relation between the Kirchhoff τ and the first Piola–Kirchhoff $\boldsymbol{T}$ stress tensors: $\tau = \boldsymbol{F}\boldsymbol{T}$, the following expressions for the thermal stress $\boldsymbol{H}^{\text{NEQ}}$ and viscous-damage $\dot{\boldsymbol{V}}^{\text{NEQ}}$

terms can be established:

$$\boldsymbol{H}^{\mathrm{NEQ}} = \boldsymbol{F}^{-1}\Gamma^{\mathrm{NEQ}} = \gamma^{\mathrm{NEQ}}\boldsymbol{F}^{T}, \tag{43}$$

$$\dot{\boldsymbol{V}}^{\mathrm{NEQ}} = \boldsymbol{F}^{-1}\ \dot{\boldsymbol{W}}^{\mathrm{NEQ}}. \tag{44}$$

The same procedure can be followed for the establishment of the first tangent tensor $\boldsymbol{R}^{\mathrm{EQ}}$ of equilibrium elastic element where $\dot{\boldsymbol{W}}^{\mathrm{EQ}}$ involves this time the damage effects only and $\boldsymbol{F}^{v} = \boldsymbol{I}$. It yields

$$\dot{\boldsymbol{T}}^{\mathrm{EQ}} = \boldsymbol{R}^{\mathrm{EQ}} : \dot{\boldsymbol{F}} - \boldsymbol{H}^{\mathrm{EQ}}\dot{\theta} - \dot{\boldsymbol{V}}^{\mathrm{EQ}}. \tag{45}$$

The final total rate form of the finite thermoviscoelastic material is as follows

$$\dot{\boldsymbol{T}} = \boldsymbol{R} : \dot{\boldsymbol{F}} - \boldsymbol{H}\dot{\theta} - \dot{\boldsymbol{V}}, \tag{46}$$

where $\dot{\boldsymbol{T}} = \dot{\boldsymbol{T}}^{\mathrm{NEQ}} + \dot{\boldsymbol{T}}^{\mathrm{EQ}}$, $\boldsymbol{R} = \boldsymbol{R}^{\mathrm{NEQ}} + \boldsymbol{R}^{\mathrm{EQ}}$, $\boldsymbol{H} = \boldsymbol{H}^{\mathrm{NEQ}} + \boldsymbol{H}^{\mathrm{EQ}}$, and $\dot{\boldsymbol{V}} = \dot{\boldsymbol{V}}^{\mathrm{NEQ}} + \dot{\boldsymbol{V}}^{\mathrm{EQ}}$. Constitutive equations can be obtained from (46) as specials cases in the presence/absence of damage and viscous effects.

3. Finite-strain micromechanical analysis

Finite strain HFGMC micromechanical analyses for the establishment of the macroscopic constitutive equations of various types of composites with doubly periodic microstructure undergoing large deformations have been previously reviewed by [Aboudi 2008]. These micromechanical analyses are based on the homogenization technique in which a repeating unit cell of the periodic composite can identified. This repeating unit cell represents the periodic composite in which the double periodicity is taken in the transverse $2-3$ plane, so that the axial 1-direction corresponds to the continuous direction; see Figure 1. (For a unidirectional fiber-reinforced material, for example, the 1-direction coincides with the

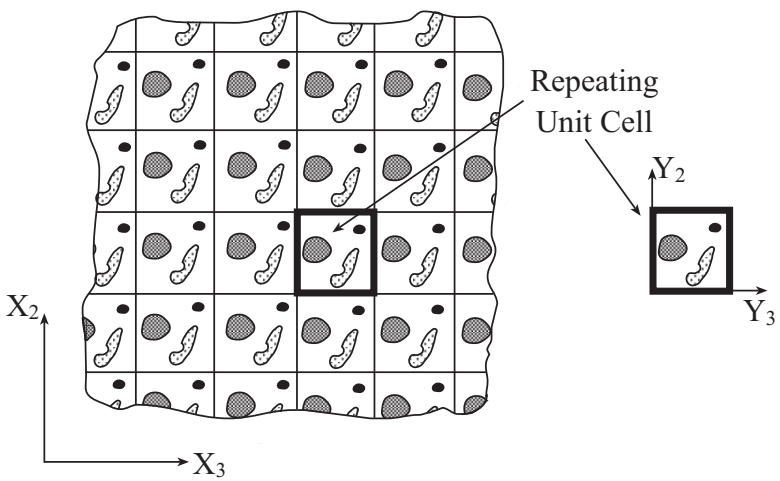

Figure 1. A multiphase composite with doubly periodic microstructures defined with respect to global initial coordinates of the plane $X_2 - X_3$. The repeating unit cell is defined with respect to local initial coordinates of the plane $Y_2 - Y_3$.

fiber orientation.) In the framework of these HFGMC micromechanical models, the displacements are asymptotically expanded and the repeating unit cell is discretized. This is followed by imposing the equilibrium equations, the displacement and traction interfacial conditions as well as the conditions that ensure that the displacements and tractions are periodic across the repeating unit cell. In particular, the imposition of the equilibrium equations provide the strong form of the Lagrangian equilibrium conditions of the homogenization theory that must be satisfied. In addition, since the solution of the repeating unit cell is determined with a constant vector, the corners of this cell are rigidly clamped to prevent this indeterminacy. The resulting homogenization derivation establishes the deformation concentration tensor $\boldsymbol{A}(\boldsymbol{Y},\theta)$, where $\boldsymbol{Y}$ are the local Lagrangian system of coordinates with respect to which field variables in the repeating unit cell are characterized. This tensor relates the rate of the local deformation gradient $\dot{\boldsymbol{F}}(\boldsymbol{Y},\theta)$ at a material point $\boldsymbol{Y}$ within the repeating unit cell to the externally applied deformation gradient rate $\dot{\bar{\boldsymbol{F}}}$ on the composite in the form

$$\dot{\boldsymbol{F}}(\boldsymbol{Y},\theta) = \boldsymbol{A}(\boldsymbol{Y},\theta) : \dot{\bar{\boldsymbol{F}}} + \boldsymbol{A}^{\mathrm{th}}(\boldsymbol{Y},\theta)\dot{\theta} + \dot{\boldsymbol{A}}^{\mathrm{vd}}(\boldsymbol{Y},\theta), \tag{47}$$

where $\boldsymbol{A}^{\mathrm{th}}$ and $\dot{\boldsymbol{A}}^{\mathrm{vd}}$ are the thermal concentration tensor and the viscous-damage contribution. The mechanical concentration tensor $\boldsymbol{A}$ is determined at every increment of loading when the thermal and viscous-damage effects are absent. Similarly, the thermal concentration tensor $\boldsymbol{A}^{\mathrm{th}}$ is determined at every increment in the absence of mechanical and viscous-damage effects. Finally, the current $\dot{\boldsymbol{A}}^{\mathrm{vd}}$ can be determined when no mechanical or thermal effects are present. It follows from (47) and in conjunction with (46) that the local stress rate at this point is given by

$$\dot{\boldsymbol{T}}(\boldsymbol{Y},\theta) = \boldsymbol{R}(\boldsymbol{Y},\theta) : \big[\boldsymbol{A}(\boldsymbol{Y},\theta) : \dot{\bar{\boldsymbol{F}}} + \boldsymbol{A}^{\mathrm{th}}(\boldsymbol{Y},\theta)\dot{\theta} + \dot{\boldsymbol{A}}^{\mathrm{vd}}(\boldsymbol{Y},\theta)\big] - \boldsymbol{H}(\boldsymbol{Y},\theta)\dot{\theta} - \dot{\boldsymbol{V}}(\boldsymbol{Y},\theta). \tag{48}$$

Hence the resulting rate form of the macroscopic constitutive equation for the multiphase thermoviscoelastic composite undergoing large deformation is given by

$$\dot{\bar{\boldsymbol{T}}} = \boldsymbol{R}^{*} : \dot{\bar{\boldsymbol{F}}} - \boldsymbol{H}^{*}\dot{\theta} - \dot{\bar{\boldsymbol{V}}}, \tag{49}$$

where $\dot{\bar{\boldsymbol{T}}}$ is the rate of the overall (global) first Piola–Kirchhoff stress tensor and $\boldsymbol{R}^{*}$ is the instantaneous effective stiffness (first tangent) tensor of the multiphase composite. It can be expressed in terms of the first tangent tensors of the constituents $\boldsymbol{R}(\boldsymbol{Y},\theta)$ and the established deformation concentration tensor $\boldsymbol{A}(\boldsymbol{Y},\theta)$ in the form

$$\boldsymbol{R}^{*} = \frac{1}{S_Y}\iint_{S_Y} \boldsymbol{R}(\boldsymbol{Y},\theta)\ \boldsymbol{A}(\boldsymbol{Y},\theta)\ dS_Y, \tag{50}$$

where S_Y is the area of the repeating unit cell. The effective instantaneous thermal stress tensor $\boldsymbol{H}^{*}$ in (49) is established from

$$\boldsymbol{H}^{*} = -\frac{1}{S_Y}\iint_{S_Y} \big[\boldsymbol{R}(\boldsymbol{Y},\theta)\ \boldsymbol{A}^{\mathrm{th}}(\boldsymbol{Y},\theta) - \boldsymbol{H}(\boldsymbol{Y},\theta)\big]\ dS_Y. \tag{51}$$

Finally, the current viscous-damage contribution to the macroscopic constitutive equations (49) is given by

$$\dot{\bar{\boldsymbol{V}}} = -\frac{1}{S_Y}\iint_{S_Y} \big[\boldsymbol{R}(\boldsymbol{Y},\theta) : \dot{\boldsymbol{A}}^{\mathrm{vd}}(\boldsymbol{Y},\theta) - \dot{\boldsymbol{V}}(\boldsymbol{Y},\theta)\big]\, dS_Y. \tag{52}$$

More details can be found in [Aboudi 2008]. It should be noted that the current values of $\boldsymbol{R}^*$, $\boldsymbol{H}^*$ and $\dot{\bar{\boldsymbol{V}}}$ of the composite are affected by the current value of damage variable through the instantaneous value of the tensors $\boldsymbol{R}(\boldsymbol{Y},\theta)$, $\boldsymbol{H}(\boldsymbol{Y},\theta)$ and $\dot{\boldsymbol{V}}(\boldsymbol{Y},\theta)$ of the finite strain constituents.

The finite strain HFGMC micromechanical model predictions were assessed and verified by comparison with analytical and numerical large deformation solutions in [Aboudi and Pindera 2004; Aboudi 2009] for composites with hyperelastic and hyperelastic coupled with damage constituents, respectively.

4. Applications

In the present section, applications are given that exhibit under various circumstances the response of a composite undergoing large deformations, which consists of a thermoviscoelastic rubber-like material reinforced by continuous thermoelastic fibers. The thermoviscoelastic matrix is characterized by the free energy functions (3) and (5) that represent elastic and maxwell elements, respectively in conjunction with the corresponding isothermal free-energy functions (11) and (12). The parameters in these functions [Reese and Govindjee 1998a] are given in Tables 1 and 2, together with η_D and $1/\eta_V = 0$ (assuming elastic bulk deformations). The damage mechanism affects the thermoviscoelastic matrix only and its parameters which appear in (22)–(24) are: $\eta_{\text{dam}} = 0.1$, $D_0^\infty = 1$ and $\alpha_{\text{dam}} = 1$. The effect of damage can be totally neglected by choosing $1/\eta_{\text{dam}} = 0$.

The continuous thermoelastic steel fibers are oriented in the 1-direction and they are characterized by the free energy function [Reese and Govindjee 1998a]

$$\psi^{\text{steel}} = \frac{(\mu_1)_{st}}{(\alpha_1)_{st}}\left[(\bar{b}_1)^{(\alpha_1)_{st}/2} + (\bar{b}_2)^{(\alpha_1)_{st}/2} + (\bar{b}_3)^{(\alpha_1)_{st}/2} - 3\right] + \frac{K_{st}}{4}\left[J^2 - 2\log J - 1\right], \tag{53}$$

where $(\mu_1)_{st}$, $(\alpha_1)_{st}$ and K_{st} are material parameters of the steel fibers which are given in Table 3. The volume fraction of the fibers is $v_f = 0.05$ which is characteristic for a rubber-like material reinforced by steel fibers.

μ_1^e (MPa)	μ_2^e (MPa)	μ_3^e (MPa)	α_1^e	α_2^e	α_3^e	K^e (MPa)	$\alpha^e(K^{-1})$	c_0^e (MPa K^{-1})
0.13790	−0.04827	0.01034	1.8	−2	7	50	223.33×10^{-6}	1.7385

Table 1. Material parameters in the function ψ_0^{EQ} of (11). The parameters μ_p^e and α_p^e, $p = 1, 2, 3$ are the Ogden's material constants, K^e is the bulk modulus, α^e is its thermal expansion coefficient and c_0^e is its heat capacity. In the small strain domain, the shear modulus of this material is 0.208 MPa.

μ_1^v (MPa)	μ_2^v (MPa)	μ_3^v (MPa)	α_1^v	α_2^v	α_3^v	K^v (MPa)	η_D (MPa s)	α^v (K^{-1})
0.3544	−0.1240	0.0266	1.8	−2	7	50	9.38105	223.33×10^{-6}

Table 2. Material parameters in the function ψ_0^{NEQ} of (12). The parameters μ_p^v and α_p^v, $p = 1, 2, 3$ are the Ogden's material constants, K^v is the bulk modulus and α^v is its thermal expansion coefficient. η_D and η_V are the viscoelastic constants with $\eta_V \to \infty$ implying elastic bulk behavior. In the small strain domain, the shear modulus of this material is 0.536 MPa.

$(\mu_1)_{st}$ (MPa)	$(\alpha_1)_{st}$	K_{st} (MPa)	$(\alpha)_{st}(K^{-1})$	$(c_0)_{st}$ (MPa K^{-1})
80769.231	2	121153.85	12×10^{-6}	3.768

Table 3. Material parameters in the function ψ^{steel} of (53). The parameters $(\mu)_{st}$ and $(\alpha)_{st}$ are the Ogden's material constants of the steel fibers, K_{st} is the bulk modulus, $(\alpha)_{st}$ its coefficient of thermal expansion and $(c_0)_{st}$ is its heat capacity. In the small strain domain, the shear modulus of the material is 80769.231 MPa.

4.1. ***The thermoelastic inversion effect.*** Consider a uniaxially stretched specimen of rubber in the 1-direction that is subjected to thermal loading (isomeric behavior). For low values of constant stretch, the graph of the gradient of the stress against temperature is negative (as in glass and metals), but becomes positive at certain critical stretching. This change of gradient sign characterizes the thermoelastic inversion effect also referred to as the Gough–Joule effect. Similarly, in ordinary materials with a prescribed stress and subjected to a thermal loading (isotonic behavior), the gradient of deformation with respect to temperature is always positive, but in rubbers this gradient becomes negative at loadings beyond a critical value. As was shown by [Ogden 1992], the derivative of the stress T_{11} with respect to the temperature θ at constant stretch λ_1: $(\partial T_{11}/\partial\theta)_{\lambda_1}$, and the derivative of the temperature θ with respect to the stretch λ_1 at constant entropy η: $(\partial\theta/\partial\lambda_1)_\eta$ (isentropic behavior) vanish simultaneously. Thus, it is possible to detect the critical value of stretch at which the thermoelastic inversion takes place by considering a strip of rubber subjected to a uniaxial stress loading under isentropic conditions, namely $\dot\eta = 0$. The minimum value of the generated temperature against applied stretch graph corresponds to the critical inversion point.

For a homogeneous material the (undamaged) entropy η_0 is given by (14). Under uniaxial stress loading in the 1-direction, the principal values b_2 and b_3 of the left Cauchy–Green deformation tensor $\boldsymbol{B}$ can be expressed in terms of the stretch $\lambda_1 = \sqrt{b_1}$ and temperature θ. Hence $\eta_0 = \eta_0(\lambda_1, \theta)$. For isentropic stretching

$$d\eta_0(\lambda_1,\theta) = \left(\frac{\partial\eta_0}{\partial\lambda_1}\right)_\theta d\lambda_1 + \left(\frac{\partial\eta_0}{\partial\theta}\right)_{\lambda_1} d\theta = 0, \tag{54}$$

where

$$\left(\frac{\partial\eta_0}{\partial\lambda_A}\right)_\theta = 2\sqrt{\frac{b_A^e}{b_A^v}}\,\frac{\partial\eta_0}{\partial b_A^e}, \qquad A = 1, 2, 3. \tag{55}$$

This relation provides

$$\frac{d\theta}{d\lambda_1} = -\frac{(\partial\eta_0/\partial\lambda_1)_\theta}{(\partial\eta_0/\partial\theta)_{\lambda_1}}. \tag{56}$$

The integration of this differential equation provides the graph of temperature deviation $\Delta\theta = \theta - \theta_0$ against the stretch λ_1 which shows initially a falling and then rising temperature, thus exhibiting the thermoelastic inversion effect. The critical value of stretch where thermoelastic inversion effect takes place correspond to the minimum of this curve.

For a rubber specimen that is subjected to prescribed stress, the critical value of the stress at which the slope of $(\partial\lambda_1/\partial\theta)_{T_{11}}$ changes sign can be determined as follows. The Maxwell relations

$$\left(\frac{\partial T_{11}}{\partial\theta}\right)_{\lambda_1} = -\left(\frac{\partial\eta_0}{\partial\lambda_1}\right)_{\theta}, \qquad \left(\frac{\partial\lambda_1}{\partial\theta}\right)_{T_{11}} = \left(\frac{\partial\eta_0}{\partial\lambda_1}\right)_{\theta} \tag{57}$$

show that $(\partial T_{11}/\partial\theta)_{\lambda_1} = 0$ yields $(\partial\eta_0/\partial\lambda_1)_{\theta} = 0$; namely, $(\partial\lambda_1/\partial\theta)_{T_{11}} = 0$. But from

$$dT_{11} = \left(\frac{\partial T_{11}}{\partial\lambda_1}\right)_{\theta} d\lambda_1 + \left(\frac{\partial T_{11}}{\partial\theta}\right)_{\lambda_1} d\theta \tag{58}$$

and (54) we obtain that $(\partial\eta_0/\partial\lambda_1)_{\theta} = 0$ implies that $(\partial\theta/\partial T_{11})_{\eta_0} = 0$. Hence the critical value of stress T_{11} can be determined from the minimum of the curve θ vs. T_{11} generated during an isentropic procedure.

In order to determine the thermoelastic inversion effect in thermoviscoelastic composites, the following tensor is defined in terms of its principal values $\partial\eta_0/\partial\lambda_p$ and unit principal directions $\boldsymbol{k}_p$, $p = 1, 2, 3$:

$$\boldsymbol{K} = \frac{\partial\eta_0}{\partial\boldsymbol{F}} = \text{diag}\left[\frac{\partial\eta_0}{\partial\lambda_1}, \frac{\partial\eta_0}{\partial\lambda_2}, \frac{\partial\eta_0}{\partial\lambda_3}\right], \quad \text{i.e.,} \quad \boldsymbol{K} = \sum_{p=1}^{3} \frac{\partial\eta_0}{\partial\lambda_p}\, \boldsymbol{k}_p \otimes \boldsymbol{k}_p. \tag{59}$$

It follows that the increment of the local value of the entropy is given by

$$\Delta\eta_0(\boldsymbol{Y},\theta) = \boldsymbol{K}(\boldsymbol{Y},\theta) : \Delta\boldsymbol{F}(\boldsymbol{Y},\theta) + P(\boldsymbol{Y},\theta)\Delta\theta, \tag{60}$$

where $P = c_0/\theta$ of the constituent. By substituting (47) in this relation the following expression is established

$$\Delta\eta_0(\boldsymbol{Y},\theta) = \boldsymbol{K}(\boldsymbol{Y},\theta) : \left[\boldsymbol{A}(\boldsymbol{Y},\theta) : \Delta\bar{\boldsymbol{F}} + \boldsymbol{A}^{\text{th}}(\boldsymbol{Y},\theta)\Delta\theta + \Delta\boldsymbol{A}^{\text{vd}}(\boldsymbol{Y},\theta)\right] + P(\boldsymbol{Y},\theta)\Delta\theta. \tag{61}$$

The increment of the global entropy of the composite is given by

$$\Delta\bar{\eta}_0 = \frac{1}{S_Y}\iint_{S_Y} \Delta\eta_0(\boldsymbol{Y},\theta)\, dS_Y. \tag{62}$$

Consider a thermoviscoelastic composite that subjected to a uniaxial stress loading in the transverse 2-direction such that all components of $\bar{\boldsymbol{T}}$ are zero except $\bar{T}_{22}$. Here, there are eight unknown deformation gradients $\Delta\bar{\boldsymbol{F}}$ (except $\Delta\bar{F}_{22}$) and $\Delta\theta$. There are, on the other hand eight equations $\Delta\bar{\boldsymbol{T}} = \boldsymbol{0}$ (except $\Delta\bar{T}_{22}$) and for isentropic procedure there is the additional relation: $\Delta\bar{\eta}_0 = 0$. Thus, the above relations enable the computation of the temperature θ that is generated at applying a transverse stretch $\bar{F}_{22}$ in a stepwise manner. Figure 2(a) shows the generated temperature deviation $\Delta\theta = \theta - \theta_0$ under isentropic and uniaxial stress loading conditions against the applied average transverse deformation gradient $\bar{F}_{22}$. This figure shows the resulting behavior of the homogeneous (unreinforced) and the unidirectional steel/rubber-like composite where the matrix is considered as thermoviscoelastic (TVE) as well as thermoelastic (TE) in which the viscous effects have been neglected. The minima of the curves correspond to the critical stretch $\bar{F}_{22}$ at which the thermoelastic inversions take place. It can be readily observed that the viscous effects on the critical points are negligible. The critical stretch of the TVE homogeneous matrix occurs at a stretch of $F_{22} = 1.023$, but due to the presence of reinforcement it moves to $\bar{F}_{22} = 1.032$. The corresponding graph which exhibits the resulting temperature deviation $\Delta\theta$ against transverse stress $\bar{T}_{22}$ is shown in Figure 2(b). This latter figure also shows the locations of the inversion thermoelastic points when the

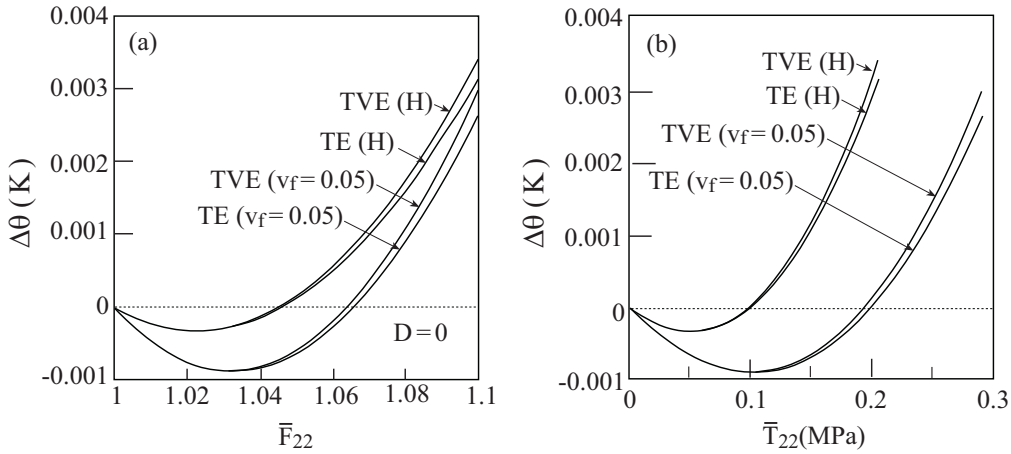

Figure 2. Temperature deviations generated by applying, under isentropic conditions, a uniaxial transverse stress loading on thermoviscoelastic (TVE) and thermoelastic (TE) composites. Also shown are the corresponding temperature deviations generated in the homogeneous (H) unreinforced matrix. The minima correspond to the locations of the thermoelastic inversions. Temperature deviations are plotted against average transverse deformation gradient (a) and against average transverse stress (b).

composite and its homogeneous unreinforced matrix are subjected to a thermal loading in conjunction with a prescribed transverse uniaxial stress. These critical stresses occur at about $\overline{T}_{22} = 0.1\,\text{MPa}$ and $T_{22} = 0.05\,\text{MPa}$ for the composite and its homogeneous matrix, respectively.

4.2. ***The composite and its unreinforced matrix responses.*** We now study the behaviors of the unidirectional thermoviscoelastic composite and its matrix under various circumstances. Figures 3 and 4

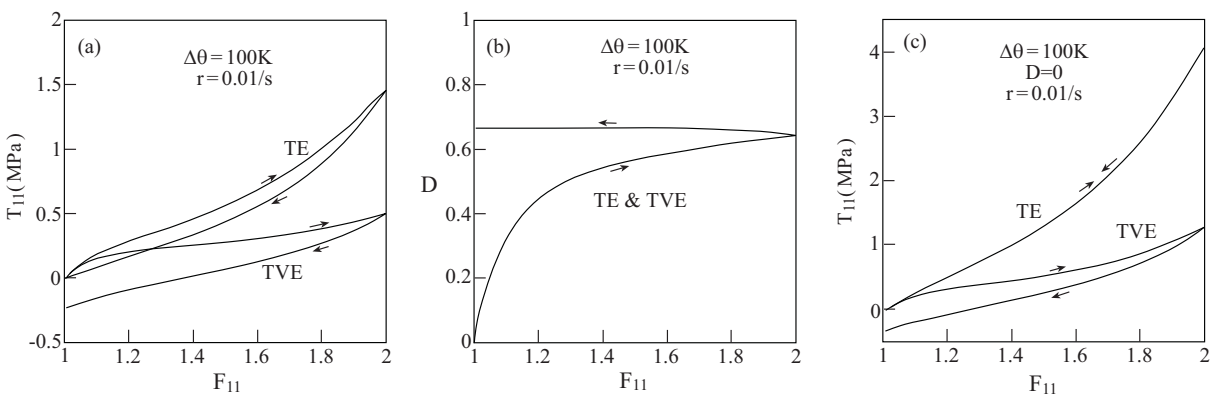

Figure 3. Response of the homogeneous thermoviscoelastic (TVE) and thermoelastic (TE) rubber-like material to uniaxial stress loading in the 1-direction, applied at elevated temperature $\Delta\theta = 100\,\text{K}$ at a rate of $r = \dot{F}_{11} = 0.01/\text{s}$: stress-deformation gradient response (a), damage evolution (b), and stress-deformation gradient response in the absence of damage (c).

show the behavior under uniaxial stress loading in the 1-direction (i.e., when all components $\boldsymbol{T}$ are zero except T_{11}) of the homogeneous (unreinforced) thermoviscoelastic (TVE) rubber-like matrix at elevated temperature $\Delta\theta = 100\,\mathrm{K}$ as well as the thermoelastic (TE) matrix when the viscous effects have been neglected. Figure 3(a) compares the response of the TE and TVE matrix, whereas Figure 3(b) shows the evolution of damage in the matrix as the loading proceeds. Here and in the following, the value of the damage refers to its maximum amount that evolves in all locations of the rubber-like phase. Figure 3(c) shows the counterpart behavior of the homogeneous matrix in the absence of any damage effects (note that the scale of the plot in the latter case is twice that of the damaged case). In all cases the rate of loading is $r = \dot{F}_{11} = 0.01/s$. This figure exhibits very well the significant viscous and damage effects on the rubber-like material behavior.

Figure 4 provides comparisons of the rubber-like material response at the reference temperature (i.e., $\Delta\theta = 0$) such that the material behavior is viscoelastic (VE), and at elevated temperature $\Delta\theta = 100\,\mathrm{K}$

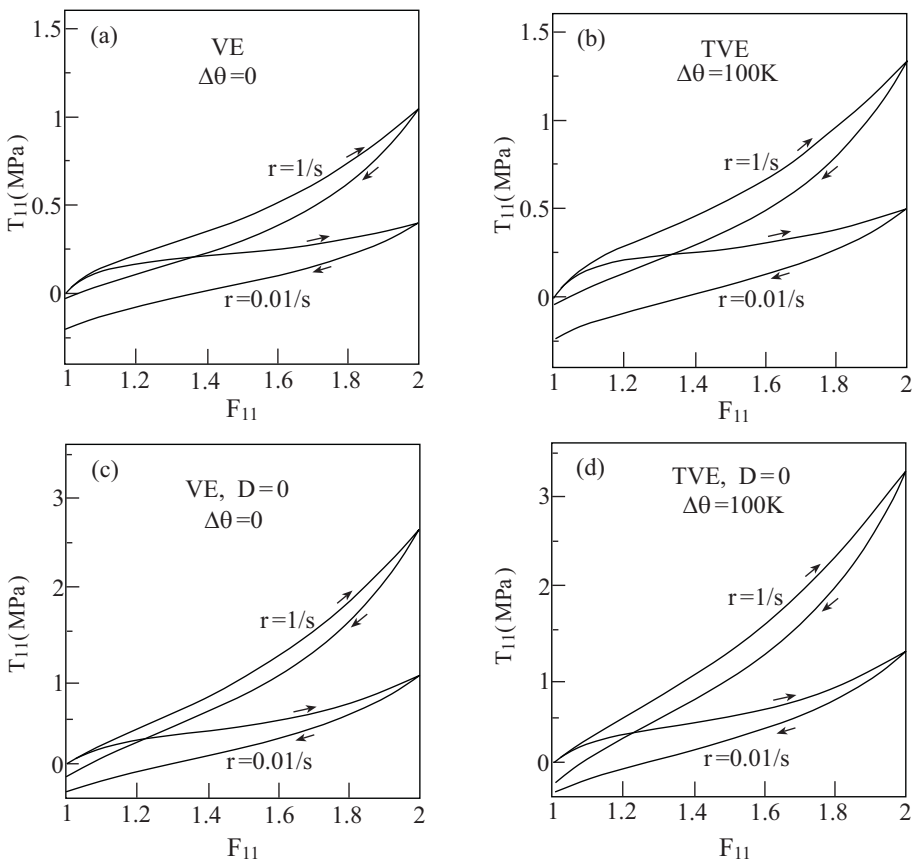

Figure 4. Top row: stress-deformation gradient response of the homogeneous viscoelastic (a) and thermoviscoelastic (b) rubber-like material to uniaxial stress loading in the 1-direction, applied at two rates: $r = \dot{F}_{11} = 1/\mathrm{s}$ and $0.01/\mathrm{s}$. In (a) the VE material is kept at $\theta = \theta_0$, in (b) the TVE material undergoes a temperature change of $\Delta\theta = 100\,\mathrm{K}$. Bottom row: corresponding results in the absence of damage effects.

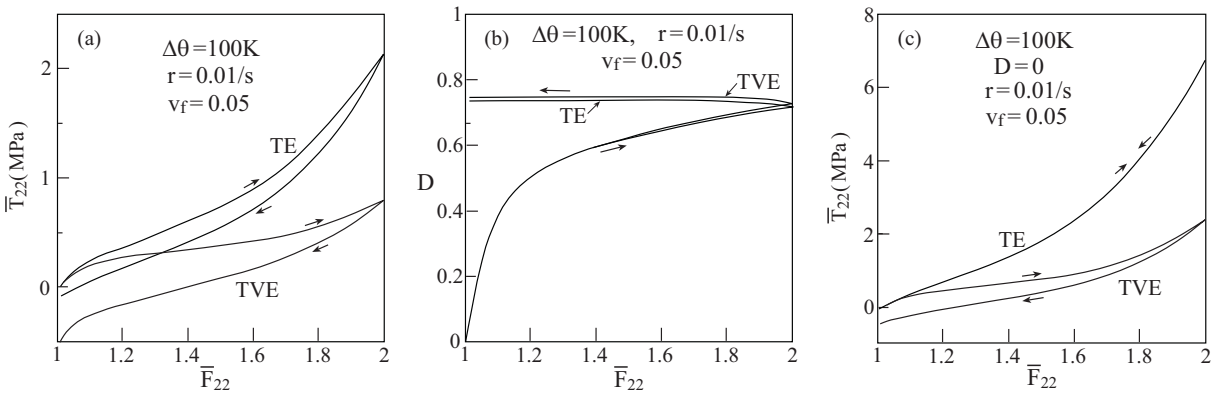

Figure 5. Response of the steel/rubber-like thermoviscoelastic (TVE) and thermoelastic (TE) composite to uniaxial stress loading in the transverse 2-direction, applied at elevated temperature $\Delta\theta = 100\,\mathrm{K}$ at a rate of $r = \dot{\bar{F}}_{22} = 0.01/\mathrm{s}$: global stress-deformation gradient response (a), damage evolution (b), and global stress-deformation gradient response in the absence of damage (c).

resulting in a thermoviscoelastic behavior (TVE). In this figure, comparisons are also shown when the uniaxial stress loading is applied at two rates $r = 1/\mathrm{s}$ and $0.01/\mathrm{s}$ in the presence and absence of damage (in the latter case the scale of the graph is twice the former). Significant differences between the various cases can be clearly observed.

Similar studies can be carried out in order to show the behavior of the unidirectional steel/rubber-like composite. In this case, the application of a transverse uniaxial stress loading perpendicular to the fiber direction is the most interesting loading, since for loading in the fiber direction (1-direction) the much stiffer elastic steel will dominate the response of the composite. In this type of loading all components of the average stress $\bar{\boldsymbol{T}}$ are equal to zero except $\overline{T}_{22}$. The transverse loading is performed by applying the average transverse deformation gradient $\bar{F}_{22}$ at a rate of $r = \dot{\bar{F}}_{22}$. Figure 5 exhibits the viscous and damage effects of the rubber-like phase on the behavior of the composite loaded at a rate of $r = 0.01/\mathrm{s}$ (note that the scale of the plot in the undamaged case is three times the damaged one). Figure 6 shows the effect of elevated temperature, rate of loading and damage on the macroscopic transverse response of the composite.

Let the unidirectional steel/rubber-like thermoviscoelastic composite be subjected to a cyclic thermal loading at a rate $\dot{\theta} = 1\,\mathrm{K/s}$ while keeping the composite traction-free ($\bar{\boldsymbol{T}} = \boldsymbol{0}$). In this thermal loading case, the temperature deviation increases/decreases linearly such that $-100\,\mathrm{K} \le \Delta\theta \le 100\,\mathrm{K}$. The resulting average of the transverse deformation gradient $\bar{F}_{22}$ caused by this thermal loading is shown in Figure 7 during 7 cycles followed by $1/4$ cycle after which the applied temperature deviation reaches $\Delta\theta = 100\,\mathrm{K}$, where the damage reaches the value of $D = 0.5$. This figure shows the transverse deformation gradient in both the presence and absence of evolving damage in the rubber-like matrix. In presence of damage, its evolution with applied thermal loading is shown in Figure 7(b). It can be readily observed that the effect of damage on the resulting transverse deformation gradient is negligible, and that the induced strains are quite small and can be regarded to belong to the infinitesimal domain. In addition, it turns out that the rate of applied thermal loading has no appreciable effect on these strains.

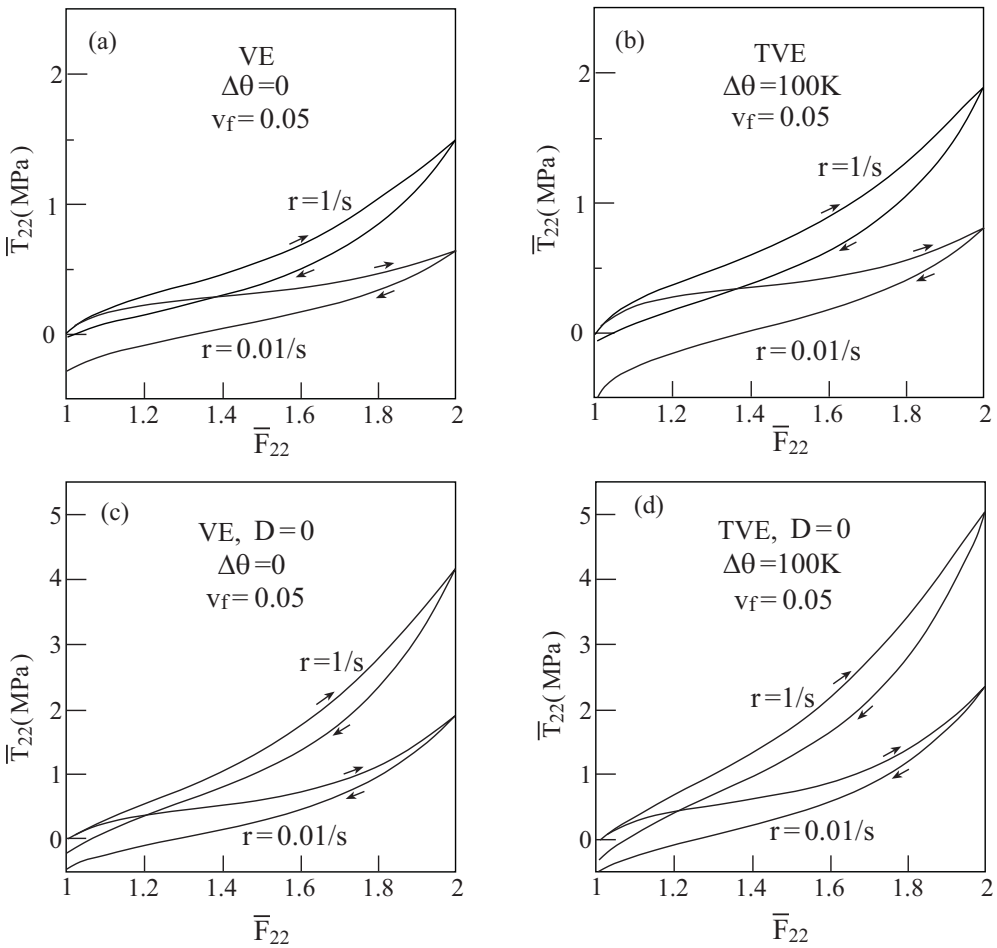

Figure 6. Top row: global stress-deformation gradient response of the steel/rubber-like viscoelastic and thermoviscoelastic composite to uniaxial stress loading in the transverse 2-direction, applied at two rates: $r = \dot{\bar{F}}_{22} = 1/\text{s}$ and $0.01/\text{s}$. In (a) the VE material is kept at $\theta = \theta_0$, in (b) the TVE material undergoes a temperature change of $\Delta\theta = 100\,\text{K}$. Bottom row: corresponding results in the absence of damage effects.

Although the previous thermal loading case that was shown in Figure 7 indicates that the effect of evolving damage on the free-thermal expansion response of the thermoviscoelastic composite appears to be minor, it should be interesting to investigate the response of the composite by applying a uniaxial transverse stress of loading and unloading at a rate of $r = \dot{\bar{F}}_{22} = 1/\text{s}$, which immediately follows the previously applied 7.25 cycles of thermal loading, $-100\,\text{K} \le \Delta\theta \le 100\,\text{K}$, which will be referred to as case 1. The response of the composite in case 1 is compared to the response which results by subjecting the steel/rubber-like composite to a uniaxial transverse stress of loading and unloading applied at a rate of $r = \dot{\bar{F}}_{22} = 1/\text{s}$ at elevated temperature $\Delta\theta = 100\,\text{K}$, referred to as case 2. The resulting comparison is shown in Figure 8 together with the evolving damage in both cases. It is readily observed that although the cyclic thermal loading ends with a damage of $D = 0.5$ in the rubber-like matrix, its effect on the

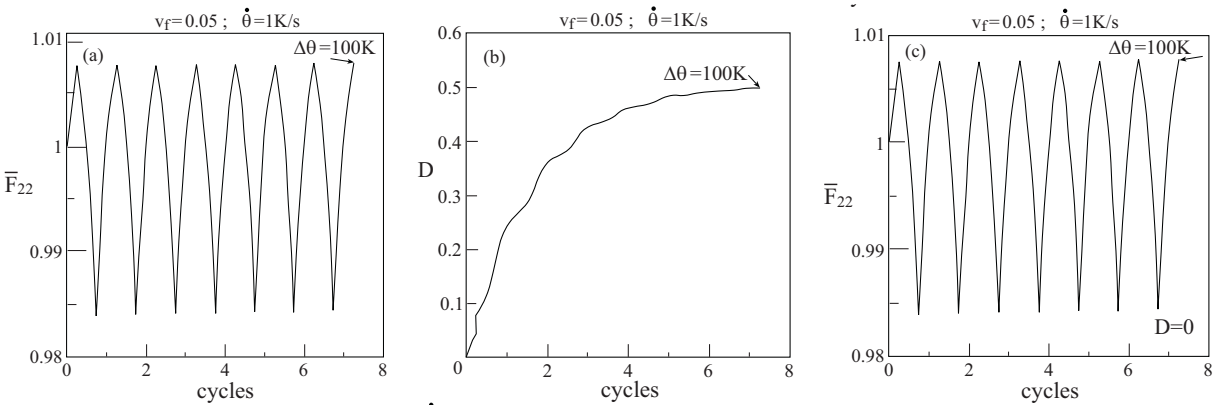

Figure 7. Response of the thermoviscoelastic steel/rubber-like composite that is subjected to cyclic thermal loading $-100\,\mathrm{K} \le \Delta\theta \le 100\,\mathrm{K}$ at a rate of $\dot{\theta} = 1\,\mathrm{K/s}$, while keeping it traction-free: transverse deformation gradient variation with cycles (a), damage evolution with cycles (b), and transverse deformation gradient variation with cycles in the absence of damage (c).

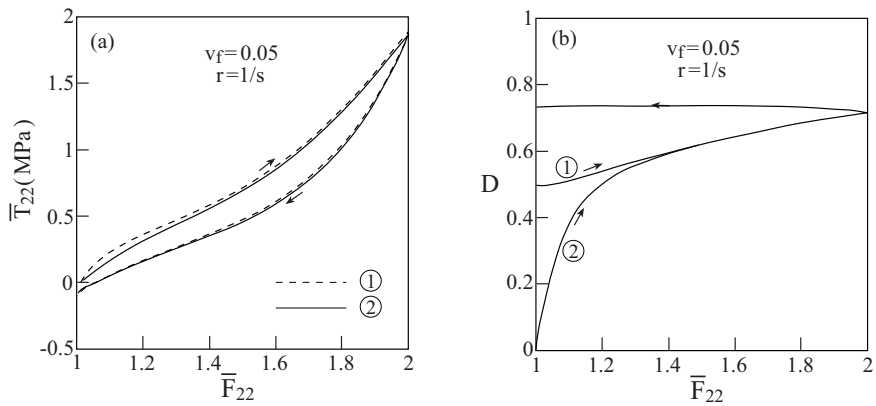

Figure 8. Response of thermoviscoelastic steel/rubber-like composite subjected to (1) cyclic thermal loading $-100\,\mathrm{K} \le \Delta\theta \le 100\,\mathrm{K}$ at a rate $\dot{\theta} = 1\,\mathrm{K/s}$, while staying traction-free, then to a uniaxial transverse stress loading-unloading, applied at a rate of $r = \dot{\bar{F}}_{22} = 1/\mathrm{s}$, at elevated temperature $\Delta\theta = 100\,\mathrm{K}$; and (2) stress loading-unloading alone, as in (1). Plot (a) shows the average transverse stress deformation gradient, plot (b) the damage evolution.

subsequent mechanical transverse loading is quite small. Applying the uniaxial transverse stress loading at the lower rate of $r = \dot{\bar{F}}_{22} = 0.01/\mathrm{s}$ gave the same closeness between the two cases.

The following four figures exhibit the creep behavior of the composite under various circumstances. Figure 9(a) compares the creep behavior of the thermoviscoelastic steel/rubber-like composite with the corresponding behavior of the homogeneous (H) matrix. In both cases a uniaxial transverse stress loading is applied at elevated temperature $\Delta\theta = 100\,\mathrm{K}$ such that all components of the stress $\bar{\boldsymbol{T}}$ are zero except $\bar{T}_{22} = 1\,\mathrm{MPa}$. Figure 9(b) shows the evolving damage to saturation in the thermoviscoelastic matrix of

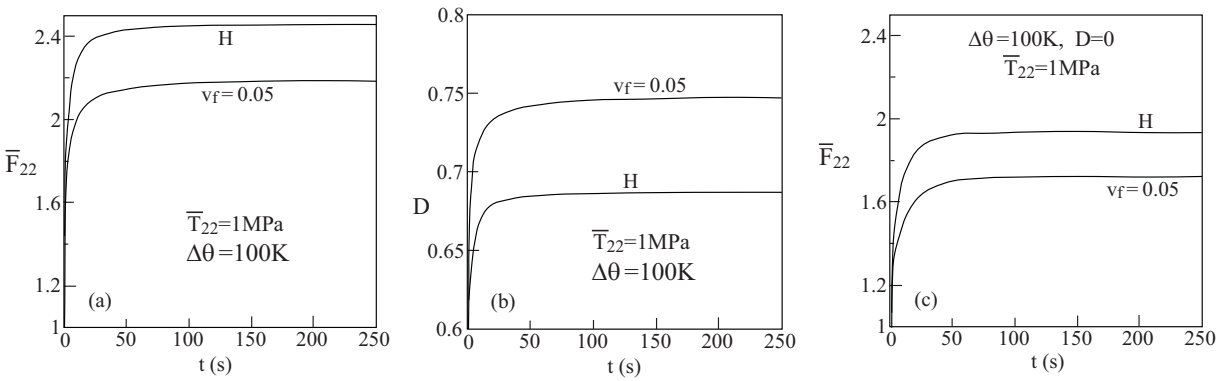

Figure 9. Creep behavior of thermoviscoelastic steel/rubber-like composite subjected to a uniaxial transverse stress loading $\overline{T}_{22} = 1$ MPa at elevated temperature $\Delta\theta = 100$ K. Also shown is the corresponding creep behavior of the homogeneous (H) unreinforced thermoviscoelastic matrix. As functions of time, the plots show the global transverse deformation gradient (a), damage evolution (b), and global transverse deformation gradient in the absence of damage effects.

the composite as well is in the unreinforced material. Finally, Figure 9(c) is the counterpart of Figure 9(a) in the absence of any damage effects.

It is interesting to observe that whereas the existence of the steel fibers decreases, as expected, the resulting macroscopic deformation gradient of the composite, the damage induced in the reinforced matrix is higher that the one that evolves in the homogeneous material. Figure 10 compares the creep behavior of thermoviscoelastic steel/rubber-like composite when it is subjected to uniaxial transverse stress loadings of $\overline{T}_{22} = 1$ MPa and 2 MPa at elevated temperature $\Delta\theta = 100$ K. This figure shows that by doubling the value of the applied stress, the global transverse displacement gradient $\overline{F}_{22} - 1$ of the

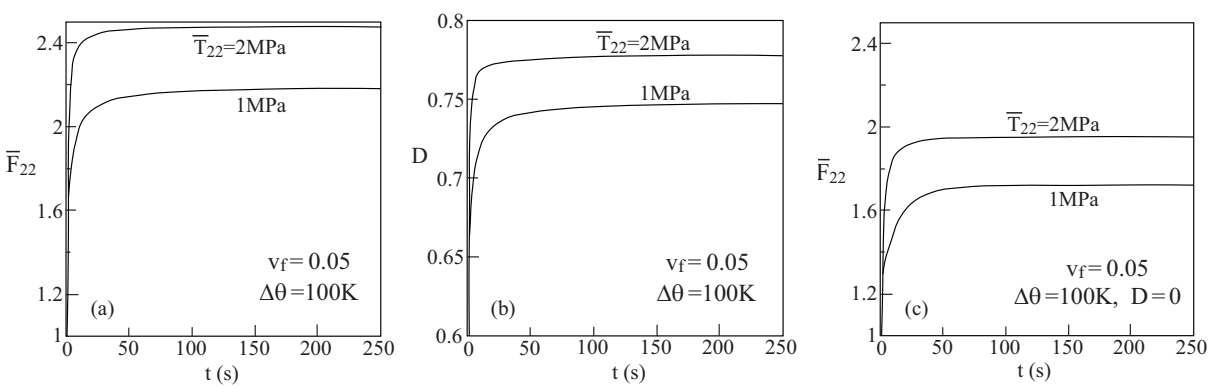

Figure 10. Comparison between the creep behaviors of the thermoviscoelastic steel/rubber-like composite which is subjected to uniaxial transverse stress loadings $\overline{T}_{22} = 1$ MPa and 2 MPa at elevated temperature $\Delta\theta = 100$ K. As functions of time, the plots show the global transverse deformation gradient (a), damage evolution (b), and global transverse deformation gradient in the absence of damage effects.

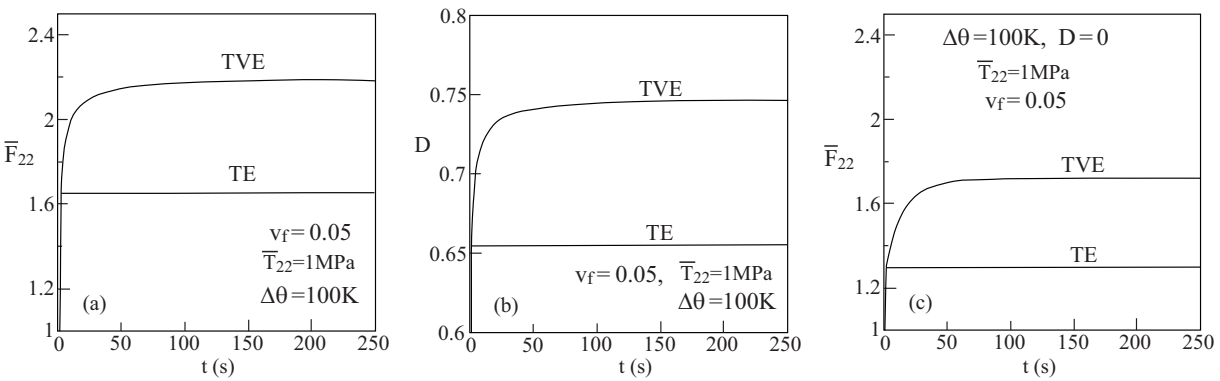

Figure 11. Comparison between the creep behaviors of thermoviscoelastic (TVE) and thermoelastic (TE) steel/rubber-like composites where in the latter the viscous effects in the matrix phase have been neglected. Both composites are subjected to uniaxial transverse stress loading $\overline{T}_{22} = 1$ MPa at elevated temperature $\Delta\theta = 100$ K. As functions of time, the plots show the global transverse deformation gradient (a), damage evolution (b), and global transverse deformation gradient in the absence of damage effects (c).

composite increases due to the nonlinearity by about 1.25 times only. On the other hand, the amount of saturation value of damage increase is just about 1.03 times. Next, Figure 11 shows the viscous effects in the matrix phase of the composite. This figure compares the creep response to uniaxial transverse stress loading $\overline{T}_{22} = 1$ MPa of the thermoviscoelastic (TVE) steel/rubber-like composite at elevated temperature $\Delta\theta = 100$ K with the corresponding thermoelastic (TE) one in which the viscoelasticity of the matrix is neglected and, therefore, there is no creep effect. The graphs show that the viscous effects are significant. It increases the saturated transverse macroscopic displacement gradient of the composite and the saturation value of damage by about 1.8 and 1.14 times, respectively. Finally, in Figure 12 the

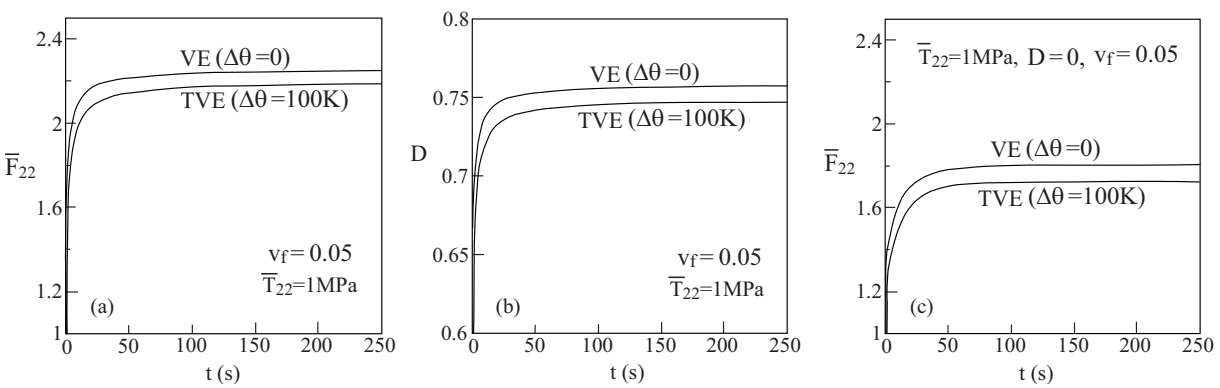

Figure 12. Comparison between the creep behaviors of thermoviscoelastic (TVE) at elevated temperature $\Delta\theta = 100$ K, and viscoelastic (VE) at the reference temperature ($\Delta\theta = 0$) of steel/rubber-like composites. Both are subjected to uniaxial transverse stress loading $\overline{T}_{22} = 1$ MPa. Global transverse deformation gradient (a), damage evolution (b), and global transverse deformation gradient in the absence of damage effects (c).

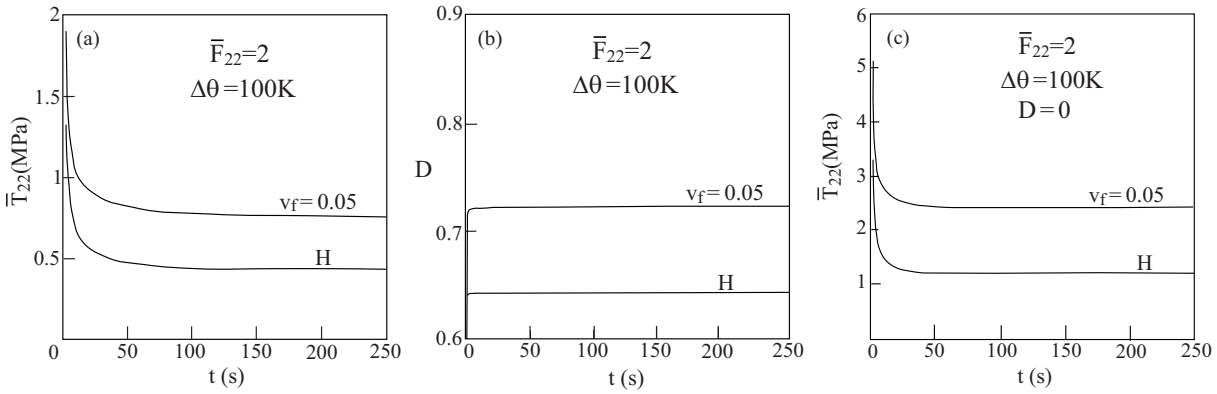

Figure 13. Relaxation behavior of the thermoviscoelastic steel/rubber-like composite which is subjected to a uniaxial transverse stress loading such that $\bar{F}_{22} = 2$ at elevated temperature $\Delta\theta = 100\,\mathrm{K}$. Also shown is the corresponding relaxation behavior of the homogeneous (H) unreinforced thermoviscoelastic matrix. Global transverse stress (a), damage evolution (b), and global transverse stress in the absence of damage effects (c).

effect of elevated temperature on the creep of the thermoviscoelastic (TVE) steel/rubber-like composite loaded by a transverse stress $\bar{T}_{22} = 1\,\mathrm{MPa}$ at $\Delta\theta = 100\,\mathrm{K}$ is compared with that of a viscoelastic (VE) composite that is subjected to the same loading but by keeping the composite at the reference temperature $\theta = \theta_0$. This figure shows that the effect of elevated temperature on the creep of the composite and the evolving damage in its matrix are not appreciable.

Corresponding to these four figures that describe the creep behavior of the composite and its matrix in various circumstances, the following four figures show the relaxation behavior of the composite and its matrix. Figure 13(a) and (c) display the relaxation at elevated temperature $\Delta\theta = 100\,\mathrm{K}$ of the thermoviscoelastic steel/rubber-like composite and its homogeneous (H) unreinforced matrix when they are subjected to a transverse deformation gradient of $\bar{F}_{22} = 2$ under uniaxial stress loading conditions (all components of $\bar{\boldsymbol{T}}$ are equal to zero except $\bar{T}_{22}$) in the presence and absence of damage effects in the matrix. (Note that the scale of the graph when $D = 0$ is three times the scale of the damaged case.) Figure 13(b) shows is the damage evolution with time. The effect of the steel fibers is well exhibited in this figure.

The effect of doubling the applied transverse displacement gradient $\bar{F}_{22} - 1$ on the relaxation behavior of the composite is displayed in Figure 14 in the presence and absence of damage (it should be noted that the scale of the plot in the latter case is four time the scale of the former one). Doubling the applied deformation gradient generates a stress at saturation of about 5.3 and 7 times in the damaged and undamaged case, respectively. The damage increases by about 1.1 times, however.

The viscous effects in the rubber-like matrix on the relaxation behavior of the composite are shown in Figure 15 at elevated temperature $\Delta\theta = 100\,\mathrm{K}$ in the presence and absence of damage. The relaxation stresses of the thermoviscoelastic (TVE) composite are observed to be much lower than the thermoelastic (TE) case in which no relaxation effects exist. In both cases, however, the viscoelasticity has a very small effect on the damage evolution in the matrix.

The final illustration is given in Figure 16, where a comparison between the relaxation behaviors of the thermoviscoelastic (TVE) composite at elevated temperature $\Delta\theta = 100\,\mathrm{K}$ and a viscoelastic (VE)

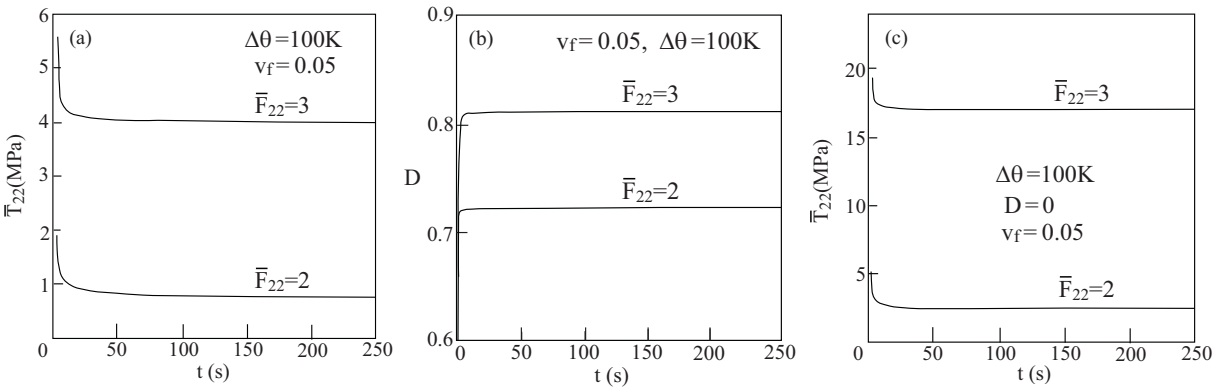

Figure 14. Comparison between the relaxation behaviors of the thermoviscoelastic steel/rubber-like composite which is subjected to uniaxial transverse stress loadings such that $\bar{F}_{22} = 2$ and 3 at elevated temperature $\Delta\theta = 100\,\mathrm{K}$. Global transverse stress (a), damage evolution (b), and global transverse stress in the absence of damage effects (c).

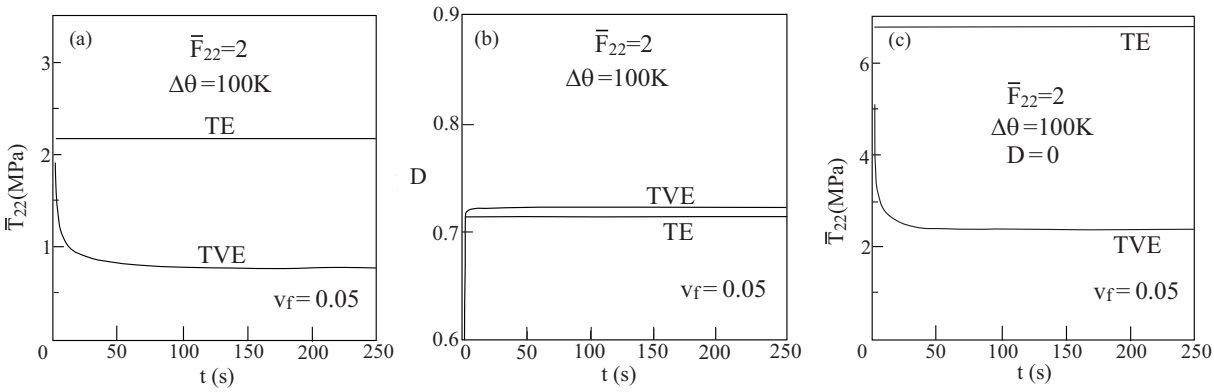

Figure 15. Comparison between the relaxation behaviors of thermoviscoelastic (TVE) and thermoelastic (TE) steel/rubber-like composites where in the latter the viscous effects of in the matrix phase have been neglected. Both composites are subjected to uniaxial transverse stress loading such that $\bar{F}_{22} = 2$ at elevated temperature $\Delta\theta = 100\,\mathrm{K}$. Global transverse stress (a), damage evolution (b), and global transverse stress in the absence of damage effects (c).

composite which is kept at the reference temperature $\theta = \theta_0$. As in the creep case, the effect of elevated temperature appears to be moderate.

Conclusions

The finite strain HFGMC micromechanical model which is capable of predicting the global behavior of thermoviscoelastic rubber-like matrix composites that are subjected to arbitrarily large thermomechanical loading has been presented. The rubber-like matrix is modeled by finite thermoviscoelasticity, which in contrast to finite linear thermoviscoelasticity where the deformations are large but the deviations from

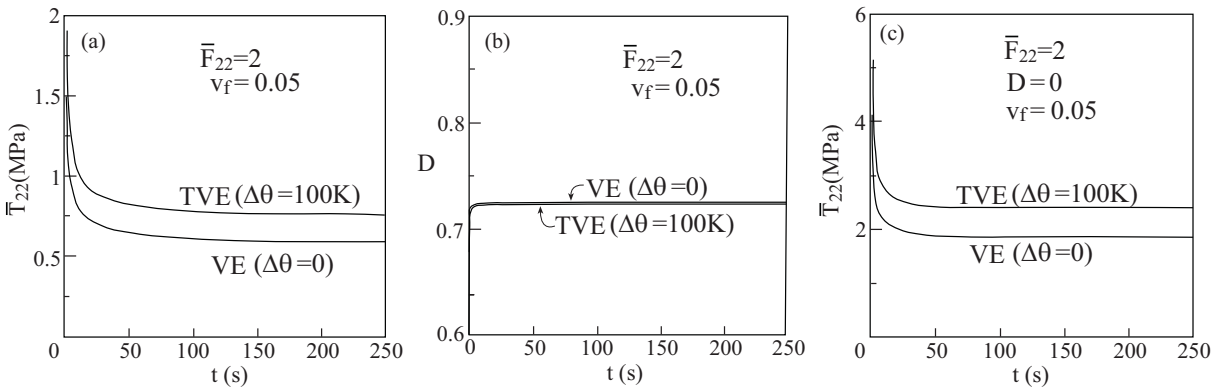

Figure 16. Comparison between the relaxation behaviors of thermoviscoelastic (TVE) at elevated temperature $\Delta\theta = 100\,\mathrm{K}$, and viscoelastic (VE) at the reference temperature ($\Delta\theta = 0$) of steel/rubber-like composites. Both composites are subjected to uniaxial transverse stress loading such that $\bar{F}_{22} = 2$. Global transverse stress (a), damage evolution (b), and global transverse stress in the absence of damage effects (c).

equilibrium are small (i.e., $\boldsymbol{B}^e \approx \boldsymbol{I}$, implying that the dependence on the strain is nonlinear but the dependence on the strain rate is linear), permits large deviation from equilibrium. In addition, the effect of evolving damage in the finite thermoviscoelastic matrix is incorporated. The finite strain HFGMC analysis establishes the rate form of the macroscopic constitutive equations that govern the composite's global response. The results exhibit the response of the composite and its unreinforced thermoviscoelastic matrix under various circumstances including their creep and relaxation behaviors.

The present derivation is confined to one-way thermomechanical coupling according to which the mechanical effects do not affect the temperature. It is possible, however, to generalize the micromechanical analysis by including a full (two-way) thermomechanical coupling.

The established global finite strain constitutive equations of the unidirectional composite can be employed to investigate the behavior of thermoviscoelastic laminates. They can be also employed to investigate the response of thermoviscoelastic structures such as laminated plates and shells undergoing large deformations. This can be performed by coupling the present micromechanical model to a finite element software such that the nonlinear composite structure response at each integration point is governed by the established macroscopic constitutive equations at each increment. This multiscale approach has been recently implemented by [Kim 2009] who coupled the hyperelastic HFGMC model to the finite element ABAQUS software in order to investigate the behavior of various types of tissue materials including the human arterial wall layers and porcine aortic valves leaflets.

References

[Aboudi 2004] J. Aboudi, "Micromechanics-based thermoviscoelastic constitutive equations for rubber-like matrix composites at finite strains", *Int. J. Solids Struct.* **41** (2004), 5611–5629.

[Aboudi 2008] J. Aboudi, "Finite strain micromechanical modeling of multiphase composites", *Int. J. Multiscale Comput. Engrg.* **6** (2008), 411–434.

[Aboudi 2009] J. Aboudi, "Finite strain micromechanical analysis of rubber-like matrix composites incorporating the Mullins damage effect", *Int. J. Damage Mech* **18** (2009), 5–29.

[Aboudi 2010] J. Aboudi, "Micromechanical modeling of viscoelastic behavior of polymer matrix composites undergoing large deformations", in *Creep and fatigue in polymer matrix composites*, edited by R. M. Guedes, Woodhead Publishing, Cambridge, UK, 2010.

[Aboudi and Pindera 2004] J. Aboudi and M.-J. Pindera, "High-fidelity micromechanical modeling of continuously reinforced elastic multiphase materials undergoing finite deformations", *Math. Mech. Solids* **9**:6 (2004), 599–628.

[Christensen 1982] R. M. Christensen, *Theory of Voscoelasticy*, Academic Press, New York, 1982.

[Cuitino and Ortiz 1992] A. Cuitino and M. Ortiz, "A material-independent method for extending stress update algorithms from small-strain plasticity with multiplicative kinematics", *Engrg. Comp.* **9** (1992), 437–451.

[Eterovic and Bathe 1990] A. L. Eterovic and K.-J. Bathe, "A hyperelastic based large strain elasto-plastic constitutive formulation with combined isotropic-kinematic hardening using the logarithmic stress and strain measures", *Int. J. Num. Meth. Engrg.* **30** (1990), 1099–1114.

[Govindjee and Reese 1997] S. Govindjee and S. Reese, "A presentation and comparison of two large deformation viscoelasticity models", *J. Engrg. Mater. Tech.* **119** (1997), 251–255.

[Holzapfel 2000] G. A. Holzapfel, *Nonlinear solid mechanics*, John Wiley & Sons Ltd., Chichester, 2000. A continuum approach for engineering.

[Holzapfel and Simo 1996] G. A. Holzapfel and J. C. Simo, "A new viscoelastic constitutive model for continuous media at finite thermomechanical changes", *Int. J. Solids Struct.* **33** (1996), 3019–3034.

[Kim 2009] H. S. Kim, *Nonlinear multiscale anisotropic material and structural models for prosthetic and native aortic heart valves*, Ph.D. dissertation, Georgia Institute of Technology, Atlanta, 2009, available at http://smartech.gatech.edu/handle/1853/29671.

[Lin and Schomburg 2003] R. C. Lin and U. Schomburg, "A finite elastic-viscoelastic-elastoplastic material law with damage: theoretical and numerical aspects", *Comput. Meth. Appl. Mech. Engrg.* **192** (2003), 1591–1627.

[Lion 1996] A. Lion, "A physically based method to represent the thermo-mechanical behaviour of elastomers", *Acta Mech.* **123** (1996), 1–25.

[Lockett 1972] F. J. Lockett, *Nonlinear viscoelastic solids*, Academic Press, New York, 1972.

[Miehe and Keck 2000] C. Miehe and J. Keck, "Superimposed finite elastic-viscoelastic stress response with damage in filled rubbery polymers: Experiments, modelling and algorithmic implementation", *J. Mech. Phys. Solids* **48** (2000), 323–365.

[Ogden 1984] R. W. Ogden, *Non-linear elastic deformations*, Ellis Horwood, Chichester, 1984.

[Ogden 1992] R. W. Ogden, "On the thermoelastic modeling of rubberlike solids", *J. Thermal Stresses* **15**:4 (1992), 533–557.

[Reese and Govindjee 1998a] S. Reese and S. Govindjee, "Theoretical and numerical aspects in the thermo-viscoelastic material behaviour of rubber-like polymers", *Mech. Time-Dependent Mater.* **1** (1998), 357–396.

[Reese and Govindjee 1998b] S. Reese and S. Govindjee, "A theory of finite viscoelasticity and numerical aspects", *Int. J. Solids Struct.* **35** (1998), 3455–3482.

[Simo 1987] J. C. Simo, "On a fully three-dimensional finite-strain viscoelastic damage model: formulation and computational aspects", *Comp. Meth. Appl. Mech. Engrg.* **60** (1987), 153–173.

[Simo 1992] J. C. Simo, "Algorithms for static and dynamic multiplicative plasticity that preserve the classical return mapping schemes of the infinitesimal theory", *Comput. Methods Appl. Mech. Engrg.* **99**:1 (1992), 61–112.

[Weber and Anand 1990] G. Weber and L. Anand, "Finite deformation constitutive equations and a time integration procedure for isotropic, hyperelastic-viscoplastic solids", *Comp. Meth. Appl. Mech. Engrg.* **79** (1990), 173–202.

Received 20 Jan 2010. Revised 1 Jun 2010. Accepted 6 Jun 2010.

JACOB ABOUDI: aboudi@eng.tau.ac.il
Faculty of Engineering, Tel Aviv University, 69978 Ramat-Aviv, Israel
http://www.eng.tau.ac.il/~aboudi/